The 13th Americas Conference on Wind Engineering (13ACWE)
Gainesville, Florida USA, May 21-24, 2017

A Preliminary Examination of Structural Fragility for a Cantilever Structure Subjected to a Thunderstorm Downburst Loading

Viet Le [a], Luca Caracoglia [a]

[a]*Northeastern University, Boston, Massachusetts, USA*

ABSTRACT: Non-stationary downburst winds can induce large-amplitude vibration on vertical slender structures. Since the physical structure of a thunderstorm is currently not fully predictable, several assumptions (modeling simplifications) and uncertainty sources (modeling errors) are present. In this paper, the propagation of errors (due to random variability) through the dynamical system and through limited knowledge of the downburst structure and loading is considered by utilizing a Monte Carlo based quasi-static simulation method for random drag coefficient. To examine the along-wind dynamic response of a simplified vertical cantilever structure, numerical integration of the linear and nonlinear dynamics is considered. The concept of structural fragility curves associated with the maximum lateral vibration of a vertical slender structure is extended to non-stationary wind loads due to thunderstorm downbursts. Furthermore, a preliminary parametric study is conducted to investigate the influence of changing factors in the downburst aerodynamic loading.

KEYWORDS: Downburst Model, Non-stationary Loads, Fragility Analysis, Performance-based Engineering, Transient Response

1 INTRODUCTION

1.1 *The downburst*

Downbursts are meteorological wind phenomena typically occurring during thunderstorms. They were first recognized by Fujita and Byers in 1977 after the investigation of several deadly aircraft accidents [1-5]. In the following decade, a significant number of aircraft accidents caused by downburst-driven wind shear were reported. Due to difficulty in physically identifying downbursts (unlike tornadoes), several on-site systematic recordings during thunderstorms were obtained by Doppler radar stations as part of projects such as the Northern Illinois Meteorological Research in Downbursts (NIMROD) in 1978 and the Joint Airport Weather Studies (JAWS) in 1982 [1, 2]. Using full-scale observations and records, meteorologists and researchers have formulated analytical models to characterize the main features of thunderstorm downburst winds [6-15]. These include a touchdown point, about which the storm is centered, a high-velocity non-stationary wind field, and a boundary layer that differs greatly from that of synoptic winds. The downburst first evolves from an intense vertical downdraft of wind that lands at a touchdown point from which it then radially diverges and decays over a short period of time. As this outburst of wind flows out from the touchdown point, the downburst travels along a path with translational velocity producing transient and non-synoptic wind fields for a short duration of time between a few to dozens of

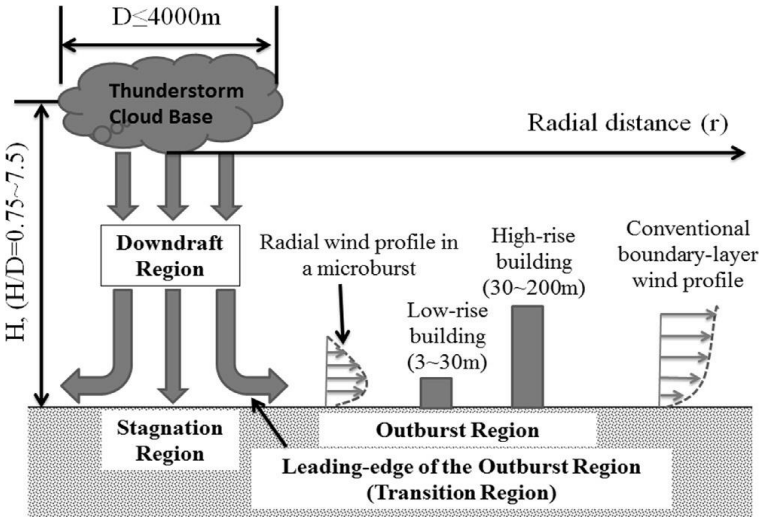

Figure 1. Schematic of a microburst – reproduced from Zhang, Sarkar *et al.* [10]

minutes. Its velocity consists of several main components: radial, vertical, horizontal, and translational [8, 9]. In addition, the velocity can be defined as a combination of a slowly varying mean wind speed and rapidly varying non-stationary turbulence. A schematic of a microburst (a type of downburst) along with a comparison between an example radial wind profile and a conventional boundary-layer wind profile is shown in Figure 1, reproduced from Ref. [10].

From a civil engineering perspective, downbursts present challenging problems as the combination of a rapidly-varying non-stationary turbulence field with a slowly-varying mean wind speed can generate complex aerodynamic loadings that lead to large amplitude vibrations. In addition, the structural response of a system under non-stationary wind loading is difficult to analyze in the frequency domain due to coupled and nonlinear equations of motions [15]. Analysis is necessary in time domain which increases computational demand or in wavelet domain which has been recently proposed. Despite these issues, research work, both through numerical analysis and physical simulation, provide insight into the importance of understanding the downburst for civil engineering applications. For example, using a transient wind simulator consisting of a 1 m diameter impinging jet with aperture control, Jesson *et al.* [16] subjected low-, mid-, and high-rise building models to conditions similar to those present in downbursts and discovered that certain building types would experience high levels of negative pressure coefficients. Le and Caracoglia [17-19] utilized the wavelet-Galerkin method to obtain the stochastic structural dynamic response of tall buildings from digitally simulated non-stationary, transient wind loadings. They selected compactly supported Daubechies wavelets and employed the Galerkin approach to transform the time-varying differential equations of motion into a discrete system of algebraic linear equations in the wavelet domain. Additional developments in techniques coupled with robust physical experimentation can aid researchers in understanding the effects that transient wind loads impose on civil engineering structures.

1.2 *Performance-based engineering*

Numerical analysis and physical simulation of non-stationary wind velocity fields typically involve various assumptions (e.g. axisymmetry of the downburst, nonevolutionary spectra of turbulence, spatial-temporal intensification functions, or pressure and load aerodynamics) due to limited

knowledge of the downburst structure and loading. Thus, significant errors from random variability accompany predictions or measurements of structural response and must be considered using probabilistic models.

Owners or engineers can use probability to establish the likelihood that a target structure may exceed a pre-defined limit state or hazard intensity. Limit states are thresholds of structural performance specified by the design criteria or intended objective [20]. Modelling this likelihood of exceedance of a limit state is an integral aspect of performance based engineering [21]. Advancements in computational structural analysis have spurred interest in the study of performance based engineering especially for the unique excitation mechanisms found in the field of wind engineering. Recent research endeavors have utilized methods such as Monte Carlo based simulations to generate fragility curves for structures under stationary wind loads [22-26].

This paper capitalizes from recent studies on the estimation of downburst-induced load and response by using Monte Carlo simulation to account for error propagation and variability in a fragility approach. A simplified vertical cantilever "point-like structure" is subjected to digitally simulated lateral downburst wind loads using a recently developed formulation for the mean wind velocity field [17-19]. In addition, turbulence is simulated with an evolutionary spectral representation methodology utilizing digital modulation to describe the time-varying downburst intensity. The linear and nonlinear dynamics of the structure are examined and fragility curves accounting for wind load variability through random drag coefficient are calculated. Furthermore, a parametric study is conducted to investigate the effects of maximum mean wind speed and distance between the downburst touchdown point and the building structure's location. The preliminary results discussed in this paper are part of an ongoing research activity oriented towards the development of a performance-based methodology for fragility analysis of the structural response due to non-stationary downburst wind loads.

2 SIMULATION OF WIND VELOCITY COMPONENTS OF DOWNBURST

2.1 *Basic structure of a downburst*

Outside the core of the downdraft, velocity features of a downburst can be described by a slowly time varying mean wind velocity (non-turbulent) and rapidly, temporally varying wind fluctuations (turbulent velocity). A simulation of the downburst wind fields typically reproduces these properties through a "deterministic-stochastic" approach, in which the turbulent and non-turbulent components are separately generated and subsequently combined through vector summation [12, 27-29]. The deterministic mean characterizes the time-varying mean wind speed while the partially coherent stochastic high-frequency fluctuation wind field describes the turbulence. This study applies a similar deterministic-stochastic approach to model the wind field. The transient horizontal downburst velocities are defined in three-dimensional space:

$$\boldsymbol{U}(x,y,z,y) = \bar{\boldsymbol{U}}(x,y,z,y) + \boldsymbol{u}'(x,y,z,t) \tag{1}$$

where the transient horizontal downburst velocity, $\boldsymbol{U}(x,y,z,t)$, is the vector sum of mean wind speed, $\bar{\boldsymbol{U}}(x,y,z,t)$, and amplitude modulated turbulence, $\boldsymbol{u'}(x,y,z,t)$.

2.2 *Slowly, time-varying mean wind velocity*

In this study, the downburst mean wind velocity, $\bar{U}_z$, profile as a function of height z is calculated with Vicroy's model [8] as shown in Equation 2.

$$\bar{U}_z(z) = 1.22\left[e^{-0.15z/z_{max}} - e^{-3.2175z/z_{max}}\right]\bar{U}_{max} \quad (2)$$

where z_{max} is the elevation from the ground at which the maximum mean wind velocity in the wind profile $\bar{U}_{max}$ occurs. Time-dependent intensification functions proposed by Chay, Albermani *et al.* [12] and Chen and Letchford [28] can then be used to generate the downburst mean wind field.

$$\bar{\boldsymbol{U}}(x,y,z,t) = \boldsymbol{U_r}(x,y,z,t) + \boldsymbol{U_{tran}}(x,y,z) \quad (3a)$$

$$U_r(x,y,z,t) = \Pi(t)\bar{U}_z(z)g(r) \quad (3b)$$

$$\Pi(t) = \begin{cases} t/t_0 & t<t_0 \\ exp(-(t-t_0)/T) & t>t_0 \end{cases} \quad (3c)$$

$$g(r) = \begin{cases} r/r_{max} & r<r_{max} \\ exp(-(r-r_{max})/R)^2) & r>r_{max} \end{cases} \quad (3d)$$

The resultant downburst mean wind velocity (slowly varying and time dependent), $\bar{\boldsymbol{U}}$, is the vector summation of the radial wind velocity, $\boldsymbol{U_r}$, and the translational velocity, $\boldsymbol{U_{tran}}$. For this study, translational wind speed is a constant 10 m/s. Radial wind velocity, U_r, is calculated using Equation 3b along with the intensification functions of Equations 3c and 3d. Equation 3c describes the evolution and intensity of the downburst through its lifecycle (Fig. 2) where t is the time since the downburst has landed at its touchdown point, t_0 is the time at which the non-turbulent velocity reaches the maximum intensity, and T is the duration of the downburst (total time of the simulation). Equation 3d represents the intensification of the downburst as a function of the horizontal radial distance, r, between the center of the downburst and the point of interest (e.g. geometric center of a building structure). At a certain location r_{max} from the core of the downburst, the intensity of the wind velocity reaches a maximum. R is the radial length scale. For the simulations in this study, various maximum mean wind velocities are used at z_{max} = 80 m while the travelling downburst has parameters t_0 = 6 minutes, r_{max} = 1000 m, and R = 700 m [30]. The duration period of the downburst, T, is 12 minutes.

The magnitude from the vector summation of Equation 3a is shown below in Equation 4.

$$\bar{\mathrm{U}}(x,y,z,t)^2 = \bar{\mathrm{U}}_r(x,y,z,y)^2 + \bar{\mathrm{U}}_{tran}(x,y,z,y)^2 + 2\times\bar{\mathrm{U}}_r(x,y,z,y)\times\bar{\mathrm{U}}_r(x,y,z,y)\times\cos\big(\beta(x,y,t)\big) \quad (4)$$

$$\cos\big(\theta(\mathrm{x,y,t})\big) = [\bar{\mathrm{U}}(\mathrm{x,y,z,y})^2 + \bar{\mathrm{U}}_{\mathrm{tran}}(\mathrm{x,y,z,y})^2 - \bar{\mathrm{U}}_{\mathrm{r}}(\mathrm{x,y,z,y})^2]/[2\times\bar{\mathrm{U}}(\mathrm{x,y,z,t})\times\bar{\mathrm{U}}_{\mathrm{tran}}(\mathrm{x,y,z,y})] \quad (5)$$

Here, β is the angle between the radial and translational velocity vectors. Equation 5 calculates the angle θ which is the deviation from the prevailing travelling direction of the storm (based on $\boldsymbol{U_{tran}}$) due to downburst mean wind speed. In this study, it coincides with the deviation from the along-wind axis due to the downburst mean wind speed.

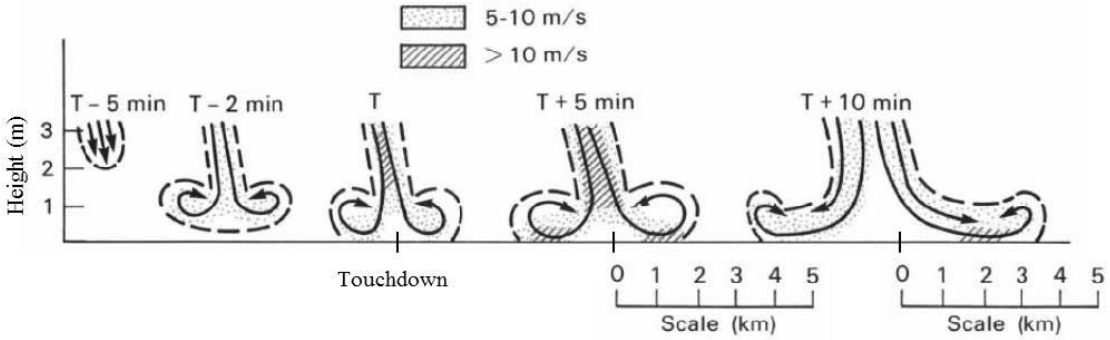

Figure 1. Schematic of the lifecycle of a downburst from touchdown to divergence – reproduced from Hjelmfelt [7].

2.3 *Rapidly, temporally varying wind fluctuations*

The partially-correlated non-stationary turbulent wind field is simulated by superposition of partially-correlated stationary processes with amplitude modulated by a slowly time-varying deterministic function [17-19]. The technique behind this approach stems from evolutionary power spectral density functions (EPSD). To simulate the one-dimensional multi-variate stationary turbulence field, Di Paola [31] has suggested the discretization of the stochastic turbulence into the superposition of single-variate, single-dimensional processes obtained through the proper orthogonal decomposition of the cross power spectral density (PSD) matrix. Using this method and the Kaimal spectrum for longitudinal wind fluctuations [32], the discretized time-dependent stochastic stationary turbulence, $u_p(x_p,y_p,z_p,t)$ at discrete locations or nodes $p = 1, 2,\ldots, M$ can be written as the following summation of M-independent processes each with frequency ω_l:

$$u_p(x_p, y_p, z_p, t) = 2\sqrt{\Delta\omega}\sum_{m=1}^{M}\sum_{l=1}^{n}\psi_{ml}\sqrt{\Lambda_m(\omega_l)}g_{ml}(t) \tag{6}$$

in which $\Delta\omega = \omega_{up}/n$ is a circular frequency interval or "step" with ω_{up} as the upper cut-off circular frequency and n as the number of circular frequencies used by the wave-superposition method. ω_l is a generic circular frequency ($\omega_l = l\Delta\omega$). ψ_{ml} is the l-th eigenvector of node p normalized with respect to the identity matrix and Λ_m represents the eigenvalues of the PSD matrix for node p. Equation 7 for $g_{ml}(t)$ represents harmonic waves of the zero-mean normal single-variate, single-dimension, processes.

$$g_{ml}(t) = R_{ml}\cos(\omega_l t) + I_{ml}\sin(\omega_l t) \tag{7}$$

R_{ml} and I_{ml} are pairs of independent, standard, normally distributed (zero expectation, unit variance) random numbers generated by the Box-Muller algorithm [33].

Turbulence amplitudes in a thunderstorm are uniformly modulated using a deterministic cosine function [34]. The modulation depends on time t but is independent of ω and the position [18]:

$$\hat{A}_p(x, y, z, t) = ((1 - \cos(2\pi t/T_0)/2)^{\eta} \tag{8}$$

T_0 is a reference duration which controls the time of maximum amplitude and η is a positive integer even number for the width of the cosine window. In this investigation, T_0 is half the time duration of the simulated downburst and η is 2. For node p, the stationary signal is at last combined with the amplitude modulation function as follows:

$$u_p^{'}(x_p, y_p, z_p, t) = \hat{A}_p(\omega, x_p, y_p, z_p, t)u_p(x_p, y_p, z_p, t) \tag{9}$$

$u_p'(x_p,y_p,z_p,t)$ is the spatially-correlated zero-mean stationary turbulence process in the same direction as the resultant downburst mean wind velocity, $\bar{U}$. This process is repeated for turbulence $v_p'(x_p,y_p,z_p,t)$ in the lateral direction perpendicular to $\bar{U}$. This component uses the Kaimal spectrum for winds in the lateral direction instead [32]. Both turbulence components, thus, are generated using spectrum models developed by Kaimal.

3 DYNAMIC RESPONSE DUE TO DOWNBURST WINDS

3.1 *Simplified, vertical cantilever, "point-like structure"*

The system is modelled after a simplified, slender, vertical cantilever structure. The "point-like structure" resembles a thin plate with an area A of 2 m^2, mass m of 6000 kg, stiffness constant k_x of 3840 N/m in the along-wind axis and k_y of 4646.4 N/m in the across-wind axis, and damping ratio ζ of 0.01. The height h of the structure is at an elevation of z = 30 m.

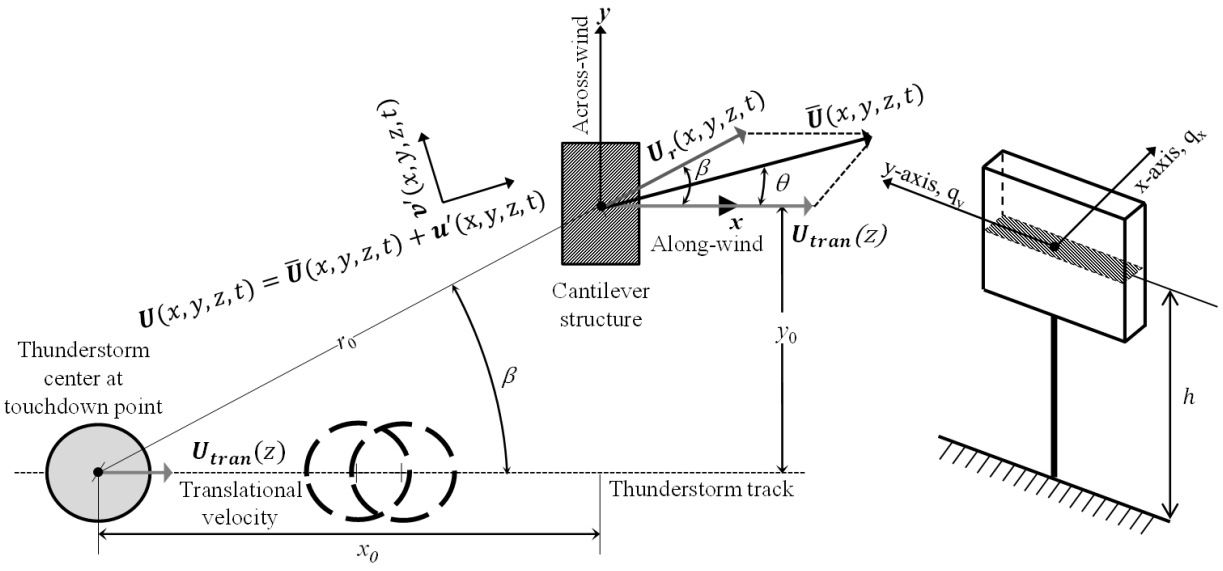

Figure 2. Schematic showing the placement of the structure with respect to the thunderstorm's path of travel. A three-dimensional view of the structure is also provided.

Two scenarios are considered for the location of the structure with respect to the storm's touchdown point. The first involves placing the structure in the path of the travelling downburst. This lends to a single degree-of-freedom (1DOF) analysis in the along-wind direction for the structural motion. The second scenario imposes an offset to the travelling downburst. The analysis is two-dimensional (2DOF) and includes turbulence and structural motion in the across-wind direction.

Figure 2 provides a schematic of the described system for the 2DOF scenario. It is assumed that the along-wind (*"x-"*) axis corresponds to the prevailing travelling direction of the storm (based on $\boldsymbol{U_{tran}}$). The local coordinate axis, perpendicular to it, is the across-wind axis (*"y-"*).

3.2 *Governing dynamic equations*

The equation dictating the time-dependent motion of the structure, *q(t)*, in the 1DOF scenario is derived from the dynamic equation of motion for a "point-like structure" subjected to a drag force (other aerodynamic forces such as transverse or lift force, moments and torque have been neglected for this study):

$$m\ddot{q}(t) + c\dot{q}(t) + k_x q(t) = \frac{1}{2}\rho U^2 A C_D \tag{10}$$

m, c, k_x are the known mass, damping, and stiffness coefficients with values given in the previous section, ρ is the air density taken as 1.25 kg/m^3, A is the area of the point (representative of a plate), C_D is the drag coefficient, and U includes the total downburst wind velocity component at time t and the effects of fluid-structure interaction.

Only for the 1DOF scenario, a nonlinear damping of the Van-der-Pol type (μ = 0.01) is introduced to study the effects of non-linearity in the structural dynamics [18]. The wind velocity, U, is calculated by the simple addition of mean wind velocity, $\bar{U}$, turbulence u', and opposing structural motion, $\dot{q}'$. After linearization to remove second-order effects of turbulence and structural motion, the differential equation of the response is given in Equation (11).

$$m\ddot{q}(t) + c(1-\mu r(t)^2)\dot{q}(t) + k_x r(t) = \tfrac{1}{2}\rho A C_D\left(\overline{U}^2 + 2\overline{U}u' - 2\overline{U}_r(t)\right) \quad (11)$$

The addition of turbulence and structural motion in the across-wind direction adds complexity to the motion equation in the 2DOF scenario. Hence, nonlinear damping has been later excluded from the formulation when a more accurate 2DOF model is considered.

The wind velocity components in the 2DOF scenario cannot simply be summed together for vector addition as is done in the simpler 1DOF case. The angle, β, between the radial velocity, U_r, and the translational velocity, U_{tran}, must be considered as shown in Equation 4 to calculate the resultant mean wind velocity, $\bar{U}$, with angle θ measured from the along-wind axis. Velocity of structural motion is first designated as follows: $\dot{q}_x$' which is parallel to $\bar{U}$ (i.e. direction denoted by angle θ) and $\dot{q}_y$' which is perpendicular to $\bar{U}$. Turbulence components, u' and as v', are also projected along the same pair of directions. The square of the magnitude of the effective velocity vector, after accounting for turbulence and structural motion (aerodynamic damping), is considered and leads to U_{eff}^2:

$$U_{eff}^2 = (U + u - \dot{q}_x'(t))^2 + (v - \dot{q}_y'(t))^2 \quad (12)$$

The terms $\dot{q}_x$' and $\dot{q}_y$' are subsequently projected onto the along-wind and across-wind axes using angle θ:

$$\dot{q}_x'(t) = \dot{q}_x(t)\,cos(\theta) + \dot{q}_y(t)sin(\theta) \quad (13)$$

$$\dot{q}_y'(t) = -\dot{q}_x(t)\,sin(\theta) + \dot{q}_y(t)cos(\theta) \quad (14)$$

A change in angle, γ, is introduced to model the fluctuation from the originally defined angle θ due to the turbulence and structural motion. It is calculated as follows:

$$\gamma = tan^{-1}\left(\left(v - \dot{q}_y'(t)\right)\Big/\left(\overline{U} + u - \dot{q}_x'(t)\right)\right) \quad (15)$$

After assuming small-angle deviations and $\bar{U}$ being significantly greater than u - $\dot{q}_x$', γ becomes:

$$\gamma = \left(v - \dot{q}_y'(t)\right)\Big/_U \quad (16)$$

The angle from the along-wind axis, at which the effective wind speed is directed, presently considers both mean wind (slowly varying) speed and turbulence fluctuations; is denoted by φ, the summation of θ and γ. The structural response in the along-wind and across-wind directions can finally be formulated by projecting the resulting drag force in the along-wind and across-wind axes shown in Figure 3. Eliminating second-order effects from turbulence and structural motion and assuming small angles, the responses of the structure in both directions due to the travelling downburst can be found:

$$m\ddot{q}_x(t) + c_x\dot{q}_x(t) + k_x q_x(t) = \tfrac{1}{2}\rho A C_D\left(\overline{U}^2 + 2\overline{U}u' - 2\overline{U}\left(\dot{q}_x(t)\,cos(\theta) + \dot{q}_y(t)sin(\theta)\right)\right)cos(\varphi) \quad (17)$$

$$m\ddot{q}_y(t) + c_y\dot{q}_y(t) + k_y q_y(t) = \tfrac{1}{2}\rho A C_D\left(\overline{U}^2 + 2\overline{U}u' - 2\overline{U}\left(\dot{q}_x(t)\,cos(\theta) + \dot{q}_y(t)sin(\theta)\right)\right)sin(\varphi) \quad (18)$$

3.3 *Random simulation of drag coefficients*

Random perturbation, thus far, has only been introduced in the generation of the standard Gaussian amplitudes of the harmonic waves superimposed for turbulence. To account for additional error

propagation or uncertainty in the system, random simulation utilizing the Monte Carlo method is performed to produce a sample of reference drag coefficients. As summarized by Di Paola [31], "[the Monte Carlo method] mainly consists in generating sample functions having prescribed probabilistic characteristics, then for each sample function the linear or non-linear dynamic structural analysis is performed. From the time histories of the response the probabilistic analysis is made on the sample functions of the response for ensuring overall safety of the various elements of the structure."

Monte Carlo methods have been previously employed in fragility and expectancy costs studies to examine wind hazards on vulnerable structures such as tall buildings and long-span bridges [23-26]. They statistically assess the dynamic response due to "uncertain loading scenarios" in which modelling simplifications and measurement errors are considered. The Monte Carlo method is used here to generate stochastic occurrences of the reference drag coefficient, C_{D0}, at the beginning of the simulation. This variable is assumed to follow a normal probability distribution with a mean of 1.2 and coefficient of variation of 0.10. These values are compatible with a large sign or support structure such as a highway sign or luminaire. If quasi-steady wind load hypothesis is used but a direction-dependent drag coefficient is introduced to simulate a non-symmetric shape in the source of aerodynamic load, this drag coefficient must be recalculated at each time instant using Equation (19) where φ is the sum of deviation from the along-wind axis due to downburst mean wind speed and turbulence fluctuations.

$$C_D = C_{D0} - 0.20(1 - cos(2\varphi)) \tag{19}$$

To linearize the wind loads, subsequent instances of drag force in time are calculated from a process utilizing the derivative of the drag coefficient with respect to angle φ. This is described below by Equation (20).

$$C_{D-lin} = C_{D0} + \left({}^{dC_D}/_{d\varphi}\Big|_{\theta} \right) \varphi \tag{20}$$

where $dC_D/d\alpha|_\theta$ is the linear rate change of the drag coefficient with respect to the angle φ, approximately evaluated at an "average" angle of attack θ (roughly coincident with the relative direction between the slowly-varying downburst velocity and the local direction x). It must be noted that Equation 20 approximates the exact relationship between relative wind angle and the local axis (orientation) of the structure. Therefore, it is only adequate for small angles only. Preliminary investigation through inspection of Equation 20 has confirmed that the approximation is acceptable in most cases and, therefore, it is used in the subsequent sections of this study. Additional investigation, beyond the scope of this paper, is under way to further examine the implications of the approximate Equation 20 on the predictions of dynamic response for point-like structures.

3.4 *Evaluating the differential equations of motion*

Approximate solutions to the differential equations can be obtained through a variety of approaches both in time and wavelet domains. This study utilizes the classic fourth order Runge-Kutta-Fehlberg (RKF) numerical integration method to approximate solutions in the time domain. For each time step that constitutes the temporal discretization, the RKF method requires information of the variables for multiple instances in the future to calculate an approximation of the integration for a differential equation. In this study, the integration result is the structural response, q, while the variables needed in the future include mean wind speed, turbulence, and deviation angle φ. The assumption of constant loads (and accelerations) during each time step of the RKF integration has been made to reduce computing time. A time step of 0.05s is used.

The time step is calibrated to minimize the influence of any modeling simplifications and to allow the elimination of second-order effects without compromising accuracy. The effect of linearization of the drag force coefficient is not fully investigated herein but may possibly be considered in future studies. Figure 3 compares the along-wind response in the 2DOF scenario produced with and without the above-described assumptions. From Equation 19, variation of the drag coefficient (0.2/1.2) may be large with respect to the angle of attack and may not be possible on a realistic structure. Responses are thus normalized by the area of the cantilever system. $\bar{U}_{max}$ is 60 m/s, x_0 is 1500 m, and y_0 is 1000 m. Drag coefficients and turbulence realizations are identical in

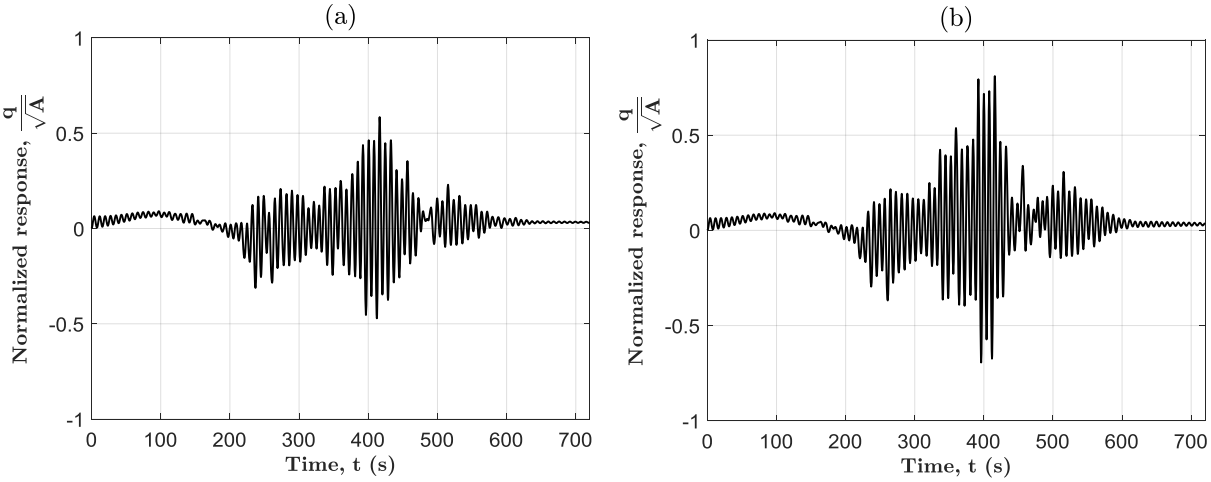

Figure 3. Example of along-wind response (a) with simplifying assumptions and (b) without any assumptions.

both cases. The results show that assumptions made for enabling numerical integration may underestimate deflections of the cantilever structure. Differences from this solution technique require further examination; this is beyond the scope of this study but must be accounted for in future investigations.

4 RESULTS AND ANALYSIS

4.1 *Parametric study*

Using the 1DOF scenario, a parametric study of x_0 is conducted for ten values: x_0 ={250 m, 500 m, 1000 m, 1500 m, 2000 m, 2500 m, 3000 m, 4000 m, 6000 m, 8000 m}; y_0 is always equal to zero (y_0 = 0 m). A sample random population of 5000 C_{D0} was generated. The quantity C_{D0} is the reference drag coefficient of the structure (zero angle of attack), which initializes the time-domain numerical integration of the differential equation of motion, Equation (11). Therefore, 5000 along-wind response sets are obtained for each value of x_0 by Monte Carlo sampling. Figure 9 shows the results for two separate downbursts with maximum mean velocities $\bar{U}_{max}$ = {40 m/s, 65 m/s} and a translational downburst velocity of U_{tran} = 10 m/s. For each distance x_0, the maximum value of the dynamic response time history is extracted. The collection of the maxima allows examination of the statistics of the response. The median, q^m_{MED}, of the sample is determined and normalized with respect to the square root of the plate's projected area, $\sqrt{A}$. The normalized median response exhibits absolute maximum at a "critical" touchdown position of x_0 = 4000 m for both velocities (Fig. 5). With x_0 = 2500 m, the structural response in Figure 5 shows a second local peak. Special

considerations must be taken to properly assess the deflection of the cantilever system at this touchdown position. A higher resolution of x_0 may perhaps reveal more cases exhibiting similar local features.

An investigation is also conducted for $\bar{U}_{max}$ using variables between 40 m/s and 65 m/s. Even though the upper limit has a less plausible physical meaning, it is selected to enable further investigation of the results. It is expected that allowing the wind field to achieve higher speeds may result in strong responses and large structural motion. Figure 5 verifies this trend. The normalized median of the maximum ${q^m}_{MED}/\sqrt{A}$ is plotted against the maximum mean wind speed of the downburst, $\bar{U}_{max}$. An exponential function is used for the empirical curve fitting of the numerical data where a and b are suitable constants.

$$q^m_{MED}\Big/\sqrt{A} = a{U_{max}}^b \tag{21}$$

At the critical touchdown point of 4000 m relative to the building center position, a downburst achieving $\bar{U}_{max}$ of 65 m/s has the potential to impose more than double the amount of structural motion in comparison with a storm that only reaches a maximum wind speed of 40 m/s. Performance-based analysis in the following section must include the increased potential for exceedance of limit states when downbursts achieve higher maximum mean wind speeds and when they land at certain critical locations.

Figure 4. Along-wind response of the benchmark cantilever structure as a function of downburst's touchdown point on the ground.

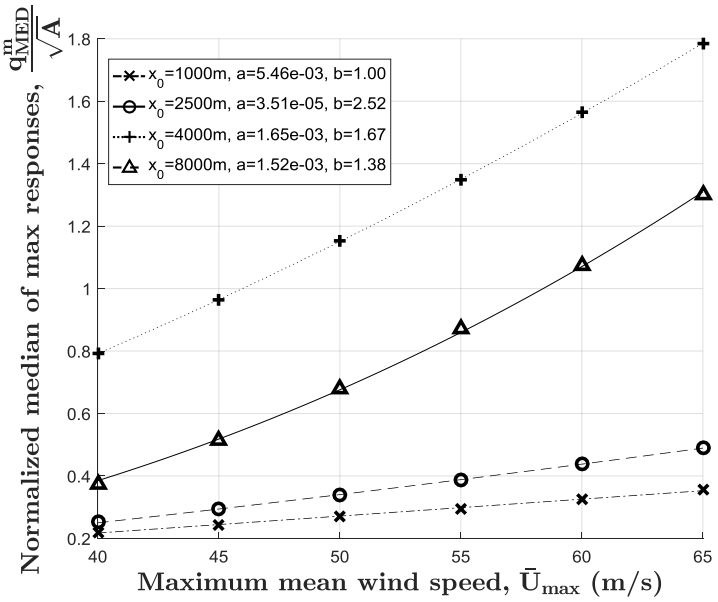

Figure 5. Examination of the empirical relationship between $\bar{U}_{max}$ and the median value of the non-stationary response maxima.

4.2 *Fragility analysis*

A parametric study is conducted to evaluate the performance of the cantilever structure against different scenarios of travelling downburst wind loads. Additionally, structural response must be examined in conjunction with the influence from a random variability or uncertainty in the wind loading [35]. This study constitutes a fragility analysis where randomization of parameters in the aerodynamic loading, such as drag coefficient and turbulence, reflects the presence of measurement or modelling errors in both in-situ wind properties and wind tunnel data variability, possible among various laboratories [36]. A typical fragility analysis includes fragility curves, estimated by determining the complementary cumulative distribution function (CCDF) that a structure will exceed a pre-defined limit state (i.e. hazard level or threshold) conditional on the reference downburst velocity (hazard intensity measure). These threshold levels can be used as indicators of structural performance, for example, by the owner or the engineer. For this study, three limit states, T_i, are defined as fractions of the height, h, of the cantilever structure. In the absence of either a specific standard or design recommendations for downburst winds, the proposed T_i values are a preliminary attempt at defining realistic thresholds for structural motion that apply to a full-scale "point-like structure" (or building), subjected to winds induced by a downburst.

$$\{T_1, T_2, T_3\} = h * \left\{\frac{1}{50}, \frac{1}{100}, \frac{1}{200}\right\} = \{0.6 \text{ m}, 0.3 \text{ m}, 0.15 \text{ m}\} \quad (22)$$

The CCDF, F_T, of the maximum structural motion, q_{max}, exceeding these limit states is represented as a function of the maximum downburst "mean" wind speed, $\bar{U}_{max}$. It is numerically determined by finding the probability, P, that a generic random variable $X = q_{max}$ exceeds the thresholds set by Equation (22), conditional on the presence of a downburst with $V_z = \bar{U}_{max}$.

$$F_T(\bar{U}_{max}) = P[X > T_i | V_z = \bar{U}_{max}] \quad (23)$$

The calculated fragility curves are approximations of the probability that the cantilever system's structural motion will exceed a limit state (i.e. threshold) when exposed to an incoming, travelling system with maximum mean wind speed, $\bar{U}_{max}$.

Figure 6 illustrates two examples of fragility curves approximated from the maximum structural responses selected from simulations where U_{tran} = 10 m/s. The interval of maximum mean wind speeds between 40 m/s and 65 m/s coincides with medium to extremely severe wind velocities for a downburst. Additional simulation sets are generated at lower velocities to ensure proper curve fitting. The log-normal cumulative distribution function (CDF) is selected to model the fragility curves due to a relative simplicity, in a linear least-squares regression, to determine the appropriate model parameters. The fragility curves approximated from Equation (23) are modelled as follows using the log-normal CDF, Φ, with *erf* as the error function, μ as the location parameter, and σ as the scale parameter [37]:

$$\Phi(\bar{U}_{max}) = {}^{1}/_{2}\left[1 + erf\left({}^{ln(\bar{U}_{max}) - \mu}/_{\sqrt{2}\sigma}\right)\right] \tag{24}$$

Additional simulations with lower maximum mean wind speeds between 5 and 35 m/s are needed for proper fitting.

As the limit states become more stringent (i.e. lower in magnitude), the probability of exceedance increases for the same $\bar{U}_{max}$ value. In addition, the downburst, when landing at x_0 = 4000 m from the building center position as opposed to x_0 = 1500 m, will have a much higher likelihood of exceeding a limit state at the same $\bar{U}_{max}$. This finding is corroborated by the results of the previously conducted parametric study, in which the median of the normalized maximum responses is greatest at x_0 = 4000 m for a downburst translating with speed U_{tran} = 10 m/s. In a practical application, an engineer or an owner may gauge the likelihood that a structural design exceeds a given threshold, established to meet requirements such as human comfort or secondary system sensitivity. Additional parameters may be incorporated in the fragility analysis and more simulations sets will increase the resolution of the curves. Furthermore, this example of performance-based thunderstorm load and response analysis can be extended to other structural models subjected to a wider range of downburst cases.

For the 2DOF scenario, the touchdown point of the downburst is offset in the across-wind direction by 1000 m (y_0 = 1000 m). The same six maximum mean wind speeds are used for the Monte Carlo simulations with random reference drag coefficient. Additional simulation sets are generated to develop the fragility curves as a function of a wider range of maximum mean wind speeds from 5 m/s to 100 m/s. The curves are once again fitted with a log-normal CDF. The results in both along-wind and across-wind directions are shown in Figure 7. In the along-wind direction, the more stringent limit state (T_3) has a higher likelihood of being exceeded than in the across-wind direction. For limit states T_1 and T_2, the opposite is true since the probabilities of exceedance in the along-wind direction more gradually increase than the one in the across-wind direction. In addition, the slopes of these two curves can be associated with a measure of the uncertainty in the structural behavior for a given threshold [38]. The steeper increments (greater slope) in probability of exceedance for the curves in the across-wind direction indicate more structural uncertainty for the cantilever system. Compared to the structural motion in the along-wind direction, a smaller variation in $\bar{U}_{max}$ can cause the structure to deflect beyond any threshold in the across-wind direction. The tighter cluster of the curves demonstrates that the system has a diminished aptitude in controlling structural motion beyond an initial sign of deflection exceedance. Further investigation is needed to evaluate fragility curves under a wider variety of conditions (e.g. varying U_{tran}, x_0, y_0, or even building type). A more efficient means for calculating structural responses while maintaining a sufficiently large sample size thus becomes a crucial task, if fragility analysis is to be implemented for broader cases.

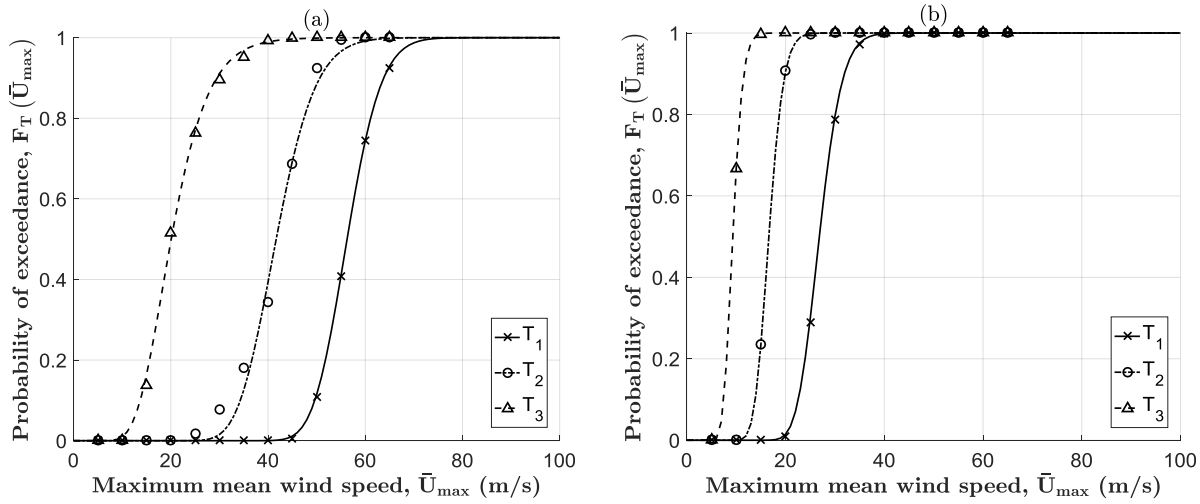

Figure 6. Fragility curves for the 1DOF scenario for (a) x_0 = 1500 m and for (b) x_0 = 4000 m.

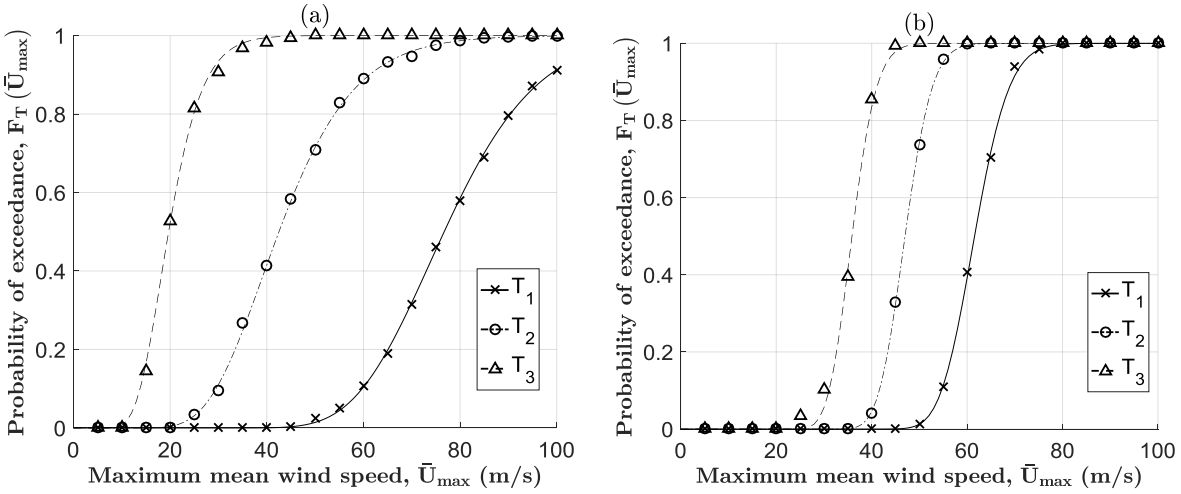

Figure 7. Fragility curves for the 2DOF scenario for (a) along-wind response and (b) across-wind response (x_0 = 1500 m and y_0 = 1000 m).

5 CONCLUSIONS AND FUTURE STUDIES

Recent implementation of fragility analysis for non-stationary wind response of a "point-like structure", subject to thunderstorm downburst winds is presented. A benchmark vertical cantilever "point-like structure" at an elevation of 30 m is digitally subjected to simulated transient wind velocity fields. The structural responses are determined by Runge-Kutta-Fehlberg (RKF) 4th order method and numerical integration of the differential equations of motion for single degree-of-freedom and two degree-of-freedom systems. Error propagation and random variability are simulated through a Monte Carlo sampling approach for the reference drag coefficient and through random Gaussian variables in the synthetic generation of non-stationary turbulence. The main findings from this study are as follows: (i) Utilizing time-dependent intensity functions, the mean wind velocity field of a travelling downburst can be digitally simulated. Turbulent wind fluctuations are

replicated with an evolutionary power spectral density approach, involving proper orthogonal decomposition of the power spectral density matrix and amplitude modulation using a cosine function. (ii) Simplifications made to enable RKF numerical integration of a large population of synthetically-generated downburst events, along with linearization of second-order terms in the wind loads, is found to underestimate results for structural response. Other methods for the solution of the differential equations of motion, which are less computationally demanding, must be investigated to avoid these assumptions. Additional investigation for direction-dependent drag forces is required since wind direction may significantly vary due to the downburst radial profile. (iii) A parametric study demonstrates the influence of relative distance between downburst and structure and maximum wind velocity on the stochastic structural response. Certain combinations between these two parameters result in considerable increments in the structural dynamic motion. (iv) Lastly, fragility analysis in both single and two degree-of-freedom scenarios shows promising potential as a feasible approach in the design of a simplified vertical structure subjected to downburst wind loading to meet selected limit states. Probabilities of exceedance of limit states are determined as a function of maximum "mean" wind speed of the downburst, used as intensity measure.

Future investigations may include more rigorous structural analysis modeling that considers across-wind and torsional responses. In addition, the fragility analysis can be expanded to more complex loadings and building models. This may require implementation of innovative techniques to determine accurate values of the structural response while utilizing less computing resource. Finally, additional parametric studies are still needed to clarify the effects of other factors such as the continuous variation in the wind direction with time, downburst translational velocity, or variable turbulence intensity of the wind field.

6 ACKNOWLEDGEMENTS

This material is based upon work supported by the National Science Foundation of the United States (NSF), under CMMI-1434880 award. Any opinions, findings and conclusions or recommendations are those of the authors and do not necessarily reflect the views of the NSF.

7 REFERENCES

1 T.T. Fujita, The downburst: microburst and macroburst, (1985).
2 T.T. Fujita, DFW microburst on August 2, 1985. 1986: University of Chicago.
3 National Transportations Safety Board (NTSB). Aircraft Accident Report--Delta Air Lines, Inc., Lockheed L-1011-385-1, N726DA, Dallas/Fort Worth International Airport, Texas, August 2, 1985, 1985: Washington, D. C. NTSB-AAR-76-8. PB86-910406.
4 National Transportation Safety Board (NTSB). Aircraft Accident Report -- Eastern Air Lines, Inc., Boeing 727-225 John F. Kennedy International Airport Jaimaica, New York. June 24, 1975, 1975. NTSB-AAR-76-8.
5 National Transportations Safety Board (NTSB). Aircraft Accident Report--Pan American Wrold Airways, Clipper 759, N4737, Boeing 727-235, New Orleans International Airport, Kenner, Louisiana, July 9, 1982, 1982: Washington D.C. NTSB/AAR-83/02. PB83-910402.
6 J.W. Wilson, et al., Microburst wind structure and evaluation of Doppler radar for airport wind shear detection, Journal of Climate and Applied Meteorology, 23 (6) 898-915 (1984).
7 M.R. Hjelmfelt, Structure and life cycle of microburst outflows observed in Colorado, Journal of Applied Meteorology, 27 (8) 900-927 (1988).
8 D.D. Vicroy, A simple, analytical, axisymmetric microburst model for downdraft estimation, (1991).
9 R.M. Oseguera and R.L. Bowles, A simple, analytic 3-dimensional downburst model based on boundary layer stagnation flow, NASA Technical Memorandum, (1988).

10 Y. Zhang, P. Sarkar, and H. Hu, An experimental study on wind loads acting on a high-rise building model induced by microburst-like winds, Journal of Fluids and Structures, 50 547-564 (2014).
11 E.-S. Abd-Elaal, J.E. Mills, and X. Ma, Empirical models for predicting unsteady-state downburst wind speeds, Journal of Wind Engineering and Industrial Aerodynamics, 129 49-63 (2014).
12 M.T. Chay, F. Albermani, and R. Wilson, Numerical and analytical simulation of downburst wind loads, Engineering Structures, 28 (2) 240-254 (2006).
13 H. Hu, Z. Yang, and P. Sarkar, Dynamic wind loads and wake characteristics of a wind turbine model in an atmospheric boundary layer wind, Experiments in Fluids, 52 (5) 1277-1294 (2012).
14 D.K. Kwon and A. Kareem, Gust‐Front Factor: A New Framework for Wind Load Effects on Structures, Journal of Structural Engineering, 5 (2009).
15 A. Kareem and T. Wu, Wind-induced effects on bluff bodies in turbulent flows: Nonstationary, non-Gaussian and nonlinear features, Journal of Wind Engineering and Industrial Aerodynamics, 122 21-37 (2013).
16 M. Jesson, et al., Aerodynamic forces on the roofs of low-, mid- and high-rise buildings subject to transient winds, Journal of Wind Engineering and Industrial Aerodynamics, 143 42-49 (2015).
17 T.-H. Le and L. Caracoglia, Coupled dynamic response of a tall building in a simulated thunderstorm downburst. in Proceedings of the 14th International Conference on Wind Engineering (ICWE14). 2015. p. 21-26.
18 T.-H. Le and L. Caracoglia, Reduced-order wavelet-Galerkin solution for the coupled, nonlinear stochastic response of slender buildings in transient winds, Journal of Sound and Vibration, 344 179-208 (2015).
19 T.-H. Le and L. Caracoglia, Wavelet-Galerkin analysis to study the coupled dynamic response of a tall building against transient wind loads, Engineering Structures, 100 763-778 (2015).
20 Eurocode-Basis of structural Design. 2002, European Committee for Standardization.
21 B.R. Ellingwood, et al., Fragility Assessment of Light-Frame Wood Construction Subjected to Wind and Earthquake Hazards, Journal of Structural Engineering, 130 (12) 1921-1930 (2004).
22 B.R. Ellingwood and P.B. Tekie, Wind load statistics for probability-based structural design, Journal of Structural Engineering, 125 (4) 453-463 (1999).
23 W. Cui and L. Caracoglia, Simulation and analysis of intervention costs due to wind-induced damage on tall buildings, Engineering Structures, 87 183-197 (2015).
24 M.A. Smith and L. Caracoglia, A Monte Carlo based method for the dynamic "fragility analysis" of tall buildings under turbulent wind loading, Engineering Structures, 33 (2) 410-420 (2011).
25 R. Bashor and A. Kareem, Probabilistic Performance Evaluation of Buildings: An Occupant Comfort Perspective. in 12th International Conference of Wind Engineering. 2007. Cairns, Australia. p. 1-6.
26 D.-W. Seo and L. Caracoglia, Estimating life-cycle monetary losses due to wind hazards: Fragility analysis of long-span bridges, Engineering Structures, 56 1593-1606 (2013).
27 M.T. Chay, R. Wilson, and F. Albermani, Gust occurrence in simulated non-stationary winds, Journal of Wind Engineering and Industrial Aerodynamics, 96 (10-11) 2161-2172 (2008).
28 L. Chen and C.W. Letchford, A deterministic–stochastic hybrid model of downbursts and its impact on a cantilevered structure, Engineering Structures, 26 (5) 619-629 (2004).
29 Y.L. Xu and J. Chen, Characterizing Nonstationary Wind Speed Using Empirical Mode Decomposition, Journal of Structural Engineering, 130 (6) 912-920 (2004).
30 J.D. Holmes and S.E. Oliver, An empirical model of a downburst, Engineering Structures, 22 (9) 1167-1172 (2000).
31 M. Di Paola, Digital simulation of wind field velocity, Journal of Wind Engineering and Industrial Aerodynamics, 74-76 91-109 (1998).
32 J. Kaimal, et al., Spectral characteristics of surface‐layer turbulence, Quarterly Journal of the Royal Meteorological Society, 98 (417) 563-589 (1972).
33 C.P. Robert, Monte carlo methods. 2004: Wiley Online Library.
34 G. Solari, Thunderstorm response spectrum technique: Theory and applications, Engineering Structures, 108 28-46 (2016).
35 L. Caracoglia, Comparison of Reduced-Order Models to Analyze the Dynamics of a Tall Building under the Effects of Along-Wind Loading Variability, ASCE-ASME Journal of Risk and Uncertainty in Engineering Systems, Part A: Civil Engineering, 2 (2) C4015002 (2016).
36 W.H. Melbourne, Comparison of measurements on the CAARC standard tall building model in simulated model wind flows, Journal of Wind Engineering and Industrial Aerodynamics, 6 (1-2) 73-88 (1980).

37 E. Weisstein. *Log Normal Distribution*. [Webpage]; Available from: http://mathworld.wolfram.com/LogNormalDistribution.html.
38 B.R. Ellingwood, LRFD: implementing structural reliability in professional practice, Engineering Structures, 22 (2) 106-115 (2000).